



HHS Public Access

Author manuscript

Glia. Author manuscript; available in PMC 2017 October 11.

Published in final edited form as:

Glia. 2016 July ; 64(7): 1154–1169. doi:10.1002/glia.22989.

Connexin 43 in Astrocytes Contributes to Motor Neuron Toxicity in Amyotrophic Lateral Sclerosis

Akshata A. Almad, Arpitha Doreswamy, Sarah K. Gross, Jean-Philippe Richard, Yuqing Huo, Norman Haughey, and Nicholas J. Maragakis

Department of Neurology, Johns Hopkins University, School of Medicine, Baltimore, Maryland

Abstract

Amyotrophic lateral sclerosis (ALS) is a neurodegenerative disease characterized by progressive loss of motor neurons in the CNS. Astrocytes play a critical role in disease progression of ALS. Astrocytes are interconnected through a family of gap junction proteins known as connexins (Cx). Cx43 is a major astrocyte connexin conducting crucial homeostatic functions in the CNS. Under pathological conditions, connexin expression and functions are altered. Here we report that an abnormal increase in Cx43 expression serves as one of the mechanisms for astrocyte-mediated toxicity in ALS. We observed a progressive increase in Cx43 expression in the SOD1^{G93A} mouse model of ALS during the disease course. Notably, this increase in Cx43 was also detected in the motor cortex and spinal cord of ALS patients. Astrocytes isolated from SOD1^{G93A} mice as well as human induced pluripotent stem cell (iPSC)-derived astrocytes showed an increase in Cx43 protein, which was found to be an endogenous phenomenon independent of neuronal co-culture. Increased Cx43 expression led to important functional consequences when tested in SOD1^{G93A} astrocytes when compared to control astrocytes over-expressing wild-type SOD1 (SOD1^{WT}). We observed SOD1^{G93A} astrocytes exhibited enhanced gap junction coupling, increased hemichannel-mediated activity, and elevated intracellular calcium levels. Finally, we tested the impact of increased expression of Cx43 on MN survival and observed that use of both a pan Cx43 blocker and Cx43 hemichannel blocker conferred neuroprotection to MNs cultured with SOD1^{G93A} astrocytes. These novel findings show a previously unrecognized role of Cx43 in ALS-related motor neuron loss.

Keywords

astrocyte; connexin; motor neuron; ALS; iPSC

Introduction

Amyotrophic Lateral Sclerosis (ALS) is an adult motor neuron (MN) disease characterized by progressive muscle atrophy, paralysis and eventual death (Ilieva et al., 2009). Transgenic mice (Bruijn et al., 1997) and rats (Howland et al., 2002) carrying mutant human SOD1

Address correspondence to Nicholas J. Maragakis, Department of Neurology, The Johns Hopkins University, School of Medicine, John G. Rangos Building, 855 North Wolfe Street, Room 248, Baltimore, MD 21205. nmaragak@jhmi.edu.

The authors do not have any conflicts of interest to declare.

genes recapitulate many, though not all, features of ALS, thus serving as a useful tool for understanding the disease.

While the clinical phenotype of ALS is primarily related to MN loss, it is now widely recognized that other neuronal subtypes are also susceptible and the clinical phenotype in some patients includes dementia (Robberecht and Philips, 2013). Other cell types, notably glial cells, contribute to MN death and associated pathology. The contribution of glial cells, like astrocytes, in toxicity to MNs has been demonstrated using co-culture studies of MNs with astrocytes from both rodents (Di Giorgio et al., 2007; Nagai et al., 2007) or human sources including post-mortem derived (Haidet-Phillips et al., 2011; Re et al., 2014), embryonic stem cell derived (Marchetto et al., 2008) or induced pluripotent stem derived cells (iPSC) (Meyer et al., 2014). Studies from mutant SOD1 chimeric mice (Clement et al., 2003) and transgenic mice (Yamanaka et al., 2008) with selective deletion of mutant SOD1 in astrocytes further display the *in vivo* contribution of astrocytes to ALS pathology. Transplantation studies conducted in our lab showed that mutant SOD1 astrocytes transplanted in cervical spinal cord of wild type rats induce focal toxicity on MNs and a decline in forelimb function (Papadeas et al., 2011).

Astrocytes form a highly coupled intercellular network in the central nervous system (CNS) through gap junctions (GJs) (Ilieva et al., 2009; Konietzko and Muller, 1994). GJs facilitate intercellular communication with exchange of metabolites (glucose, lactate), ions (K^+ , calcium), and second messengers (cAMP, IP3, ATP) (Kielian 2008). Each GJ is composed of two opposing hemichannels and each hemichannel is made of six connexin subunits arranged around a central pore (Kielian, 2008). Connexin 43 (Cx43) is the predominant connexin in astrocytes and is expressed ubiquitously in astrocytes and microglia throughout the CNS (Cotrina et al., 2001; Rochefort et al., 2005). Cx30 is the other connexin that mediates coupling of astrocyte networks (Gosejacob et al., 2011), while Cx26 and Cx40 are expressed to a lesser degree in astrocytes (Rash et al., 2001). Some of the key functions attributed to Cx43 are homeostatic buffering, synchronization of astrocyte networks, metabolic support for neurons, regulation of vascular components and modulation of synaptic activity and plasticity (Giaume and Liu, 2012).

Cx43 is mainly thought to form GJs that interconnect astrocytes. They also form a network with other cells in CNS as well. There is increasing evidence that hemichannels, the sub-component of GJs, play a role in physiological conditions and neurodegenerative diseases (Bennett et al., 2003; Orellana et al., 2009; Avendano et al., 2015; Rovegno et al., 2015). Cx43 immunoreactivity co-localizes with astrocytes within 80% of amyloid ($A\beta$) plaques of human post-mortem tissue and also co-localizes with plaques in a mouse model of Alzheimer's disease (Nagy et al., 1996). Similar increases in Cx43 expression are reported in models of stroke and retinal and cerebral ischemia where amplification of cell death signals occurs through GJs as well as models of neurotrauma such as traumatic brain injury and spinal cord injury (Chen et al., 2012; Chew et al., 2010; Sun et al., 2015; Rovegno et al., 2015). Administration of pan GJ blockers and Cx43-specific mimetic peptide blockers in these models are found to be neuroprotective and serve as potential therapeutics (Chew et al., 2010; Kerr et al., 2012).

Some studies have shown an increase in Cx43 expression in ALS rodent models (Cui et al., 2014; Diaz-Amarilla et al., 2011; Keller et al., 2011), with no change in Cx30 expression levels (Cui et al., 2014). However, the functional contribution of connexin biology in ALS is largely unexplored. In this study, we demonstrate that astrocyte Cx43 levels are increased temporally and anatomically following disease progression in the SOD1^{G93A} mouse model. This increase in Cx43 expression is notably mirrored in human ALS neural tissues and iPSC-derived astrocytes. The increased levels of Cx43 result in increased GJ and hemichannel activity in SOD1^{G93A} astrocytes. Finally, we demonstrate that modulation of Cx43 can mitigate SOD1^{G93A} mediated astrocyte toxicity to motor neurons.

Materials and Methods

Animals

Transgenic mice carrying the normal human SOD1 gene (B6SJL-Tg (SOD1) 2Gur/J), stock #002297) and the human SOD1 gene with the G93A mutation (B6SJL-Tg (SOD1*G93A) 1 Gur/J; Stock # 002726) (Lepore et al., 2007, 2008a) were used for the study. Male and female mice were obtained from The Jackson Laboratory (Bar Harbor, ME), and maintained as an in-house colony. All procedures were conducted in strict accordance with the guidelines set by the European Communities Council Directive (November 24th, 1986), the NIH Guide for the Care and Use of Laboratory Animals, the Guidelines for the Use of Animals in Neuroscience Research and the Johns Hopkins University IACUC, and measures were taken to minimize any potential pain or animal discomfort. Mice were housed at standard temperature (21°C) and in a light controlled environment with ad libitum access to the food and water, and were maintained in racks of ventilated cages located in the same room. In order to avoid dehydration, Aqua-Jel packs were provided when animals started to show disease symptoms.

Human Tissue

Human samples from control and sporadic ALS patients were obtained from the Department of Veterans Affairs, VA Biorespository. The samples obtained in the study are described in Table I.

Nanostring Analysis

NanoString (NanoString Technologies™, Inc., Seattle, WA, <http://www.nanostring.com>) analyses were performed on control and ALS human samples from motor cortex, cervical spinal cord and lumbar spinal cord. The nCounter system of NanoString allows for direct detection and counting of nucleic acid via reporter probes appended with multiple fluorophore barcodes and biotinylated capture-probes that attach to microscopic beads, which are then affixed to lanes in a translucent cartridge and read in an optical scanner. NanoString probe design and sequence information has been previously described (Haidet-Phillips et al., 2014). RNA was isolated from the above-mentioned tissues using Trizol, followed by DNase treatment and RNA cleanup using RNeasy columns (Qiagen, Hilden, Germany). Batches of 12 separate samples at one time were prepared as per manufacturer instructions, with 100 ng of total RNA hybridized with probes at 65°C for 16–18 h before being placed into the automated nCounter Prep Station (Nanostring) in which samples were

affixed to cartridges. Cartridges were then immediately placed into the nCounter Digital Analyzer (Nanostring) optical scanner and color codes on the surface of the cartridge were counted and tabulated for each target molecule. All samples were normalized using internal positive controls and three housekeeping genes (B2M, GAPDH, and OAZ1) with human-specific probes. Before normalization, all raw values reading less than 10 total counts were eliminated from the analysis because they were under the standard limit of detection. Total counts after normalization was graphed. In terms of gene expression, a “count” is referred to as a single molecule of mRNA transcript bound by the NanoString® probes.

Immunoblotting

SOD1^{G93A} mice were perfused at different stages of the disease: pre-symptomatic (60 days), symptomatic (90 days) and endstage (120–140 days) along with their littermate controls. The mice were anaesthetized using 4% hydrochlorate and perfused with cold saline. Different segments of the spinal cord were isolated and homogenized in T-PERS buffer (pH 7.6; Pierce) containing proteinase and phosphatase inhibitor. Briefly, homogenates were centrifuged and supernatants were used to measure protein concentrations. Next, 10 µg of protein was loaded and resolved by using a 4–12% Bis-Tris Nupage gel (Invitrogen) and then transferred to a nitrocellulose membrane. The membrane was blocked in 5% milk in PBS (0.1 M) for 1 h and then incubated at 4°C overnight on a shaker in the appropriate primary antibody. The next day the membrane was washed 4–5 times with 0.5% Tween in PBS and placed in an appropriate secondary antibody for 2 h at room temperature on a shaker. Next the membrane was washed and developed by using the Super Signal West pico chemiluminescent kit (Pierce). The membrane was exposed to autoradiographic X-ray films (ISC BioExpress, Kaysville, UT) or the Biorad Imager and the signal was detected. The primary antibodies used were rabbit polyclonal Connexin 43 (1:5000, Sigma C6219), mouse monoclonal GFAP (1:5000, Millipore MAB360), rabbit monoclonal Cx30 (1:500, Invitrogen 700258). All the proteins were normalized to rabbit polyclonal GAPDH (1:5000, Cell Signaling Technology 14C10), which was used as the loading control. Similarly, tissue from human post-mortem samples (control and ALS patients) were probed for Connexin 43 protein levels.

Immunohistochemistry

To examine the pathology of SOD1^{G93A} mice, we sacrificed mice at 60 days, 90 days and when they reached endstage. Mice were anesthetized and transcardially perfused first with saline and then with 4% paraformaldehyde (PFA). Brain and spinal cord were isolated and fixed overnight in 4% PFA. The tissue was rinsed with 0.2 M PB the next day and cryopreserved in 30% sucrose solution. The tissue was then frozen in tissue freezing medium and sectioned at 25 µm thickness. In brief, spinal cord sections were rinsed three times with 0.1 M PBS for 10 min each. The tissue was then blocked with 10% goat block containing 0.2% triton-X for 1 h. Sections were incubated overnight at 4°C with the relevant antibodies in 5% goat block. The next day the sections were washed in 0.1 M PBS and then incubated with the species-specific secondary antibody for 2 h at room temperature. The sections were then washed and mounted with Prolong gold with DAPI (Life Technologies) and stored until ready to image. The antibodies used were Cx43 (1:5000, Sigma C6219), chicken GFAP (1:200, Millipore AB5541) and Cx30 (1:200, Invitrogen 700258).

Immunocytochemistry for coverslips from mouse and human iPSC astrocytes were also stained using a similar protocol. Briefly, the coverslips were fixed with 4% PFA for 10 mins and then washed with 0.1 M PBS three times. Coverslips were then blocked and stained with the appropriate primary and secondary antibodies as described above. The antibodies used were rabbit Cx43 (1:200, Sigma C6219), monoclonal mouse GFAP (1:200, Millipore MAB360) and monoclonal mouse S100 β (1:500, Sigma S2532). They were mounted using Prolong gold with DAPI and imaged accordingly. All microscopic images were arranged into plates by using Adobe Photoshop.

Astrocyte Culture

Glial restricted precursors (GRPs) were isolated from embryonic mouse spinal cord at 11.5 days and cultured as previously described (Lepore et al., 2008b; Papadeas et al., 2011). GRPs were then differentiated towards astrocytes by supplementing the media with 10% FBS and then plated as needed for the experiments for about a week. The samples for immunoblotting were then collected using the T-PER buffer and tested using the method described above.

qPCR Analysis

Mouse specific primers were designed for Cx43, GFAP, and the primer sequences were confirmed by BLAST analysis for highly similar sequences against known databases and tested for specificity. RNA extraction was conducted using the trizol extraction method. The RNA was then converted into cDNA using the iScriptTM cDNA synthesis kit (Bio-Rad) as per the protocol described by the manufacturer. The cDNA was then amplified using the SYBR green PCR master mix (Applied Biosystems) and the relative gene expression of Cx43 was quantitated using the comparative C_T method.

Human iPSC Astrocyte Culture

The generation, characterization of the human iPSC lines and their differentiation into astrocytes is described previously in Haidet-Phillips et al. (2014). The information for different lines of iPSC cells are described in Table II. In brief, the protocol for the differentiation of iPS cells into astrocytes was conducted over 90 days using a dual SMAD inhibition approach involving neuralization, caudalization, ventralization and the final steps of glial differentiation into astrocytes. About 50,000 astrocytes were then plated per well in a 24-well plate to reach confluency and maintained for a week before collecting samples for protein or before fixing for immunohistochemical analysis. Immunoblotting was conducted using the methods described above and data was analyzed using Image J software.

Scrape Loading Assay

In order to assess astrocyte gap junction permeability, we conducted a scrape-loading assay with Lucifer Yellow (LY) dye as described previously by Giaume et al. (2012). In brief, a confluent layer of astrocytes was grown for one week on coverslips. On the day of assay, the cells were exposed to an ionic solution containing Ca²⁺ for about 10 min (DPBS +Ca²⁺, Life Technologies). The cells were then placed in a similar solution without Ca²⁺ for 1 min (DPBS-Ca²⁺, Life Technologies). The scrape-loading assay was then performed using a

razor blade in the same Ca^{2+} free solution (DPBS- Ca^{2+}) containing LY dye (1 mg/mL, Life Technologies, L-12926) for 5 min. After that the solution was withdrawn and the cells were washed about 8–10 times with a large volume of HEPES buffer salt solution (Life Technologies) and allowed to rest for 8 min for intracellular diffusion of the dye before fixing them for analysis. The quantification of the spread of LY dye from the scratch point was measured between $\text{SOD1}^{\text{G93A}}$ and SOD1^{WT} astrocytes ($n = 5$ coverslip/group; 3 images per coverslip was analyzed). The contribution of Cx43 mediated coupling was established with the use of a Cx43 specific peptide blocker called GAP26 (200 μM Tocris, Cat. No. 1950). The amount of dye transfer was assessed using the Image J software and reported in integrated density using arbitrary units (A.U.). The experiments were conducted independently at least three times.

Intracellular Calcium Levels

Confluent layer of astrocytes was loaded with 10 μM Fura-2 AM (cell permeable Ca^{2+} indicator, Life Technologies, F-1201) for about 20 mins along with 0.01% Pluronic® F-127 (Life Technologies, P-3000MP) at 37°C (Giaume et al., 2012). The astrocyte coverslips loaded with Fura-2 were placed in a calcium-imaging buffer (150 mM NaCl, 5 mM KCl, 1 mM MgCl_2 , 2 mM CaCl_2 , 10 mM glucose, 10 mM HEPES, pH 7.4) and transferred to the stage of a Zeiss Axiovert microscope coupled to a CCD camera and a Zeiss AttoFluor calcium imaging system. Cells were maintained at 37°C on a heated stage and were imaged using a 40X oil objective. The average concentration of Ca^{2+} in the cells was determined from the ratio of the fluorescence emissions obtained using two different excitation wavelengths (340 nm and 380 nm). A single astrocyte was mechanically stimulated with a glass pipette (1–2 μm) to induce Ca^{2+} waves. The amplitude of intracellular calcium wave propagation from stimulated to nonstimulated cell was measured at equi-distance points.

For measuring Ca^{2+} levels with ATP stimulation, the astrocytes were perfused using 10 μM ATP using a perfusion chamber and perfusion pump for 30 s and then perfused again with the calcium-imaging buffer. The amplitude of peak calcium concentration was plotted for the two genotypes and to establish the role of Cx43, the coverslips were preincubated with 200 μM of Cx43 blocker GAP26. At least three independent experiments were conducted for mechanical stimulation and for ATP stimulation with $n = 8$ –10 coverslips/group.

Hemichannel Assay

To assess hemichannel activity, ethidium bromide (EtBr) uptake was performed as described previously (Orellana et al., 2011a; Giaume et al., 2012). Astrocytes derived from SOD1^{WT} and $\text{SOD1}^{\text{G93A}}$ mice were exposed to 5 μM EtBr for 10 min at 37°C. The cells were then washed gently thrice with HBSS containing Ca^{2+} and immediately fixed with 4% PFA. The astrocytes were mounted with Prolong Gold with DAPI (Life Technology) and images were captured using a Nikon epifluorescence microscope ($n = 5$ /group, for three independent experiments). For testing effect of EtBr uptake upon cytokine stimulation, astrocytes were incubated with 10 μM of TNF- α and 10 μM of IL-1 β for 24 h at 37°C. GAP26 (200 μM) was incubated for 10 min along with EtBr to show that the hemichannel activity is mediated at least partially through Cx43 hemichannels. The amount of EtBr uptake was measured using the software ImageJ and was plotted as intensity measurements.

Astrocyte/Motor-Neuron Culture

Astrocyte motor neuron co-culture experiments were performed as described previously by Haidet-Phillips et al., 2011. Briefly, mouse ES cells that express green fluorescent protein (GFP) driven by the Hb9 promoter were differentiated to MNs as previously described (Wichterle et al., 2002). After 5 days of differentiation, the embryoid bodies were dissociated and sorted for GFP⁺ motor neurons on a FACS sorter. Three days prior to MN cell sorting, astrocytes from SOD1^{G93A} and SOD1^{WT} were plated on 96-well plates at 45,000 cells/well. FACS purified Hb9-GFP⁺ MNs were plated onto astrocytes at 10,000 cells/well in MN media as previously described (Haidet-Phillips et al., 2011). The cells were treated every other day with either 200 μ M GAP26, a Cx43 blocker, 344 μ M GAP19 (Tocris, Cat. No. 5353), a Cx43 hemichannel blocker (Abudara et al., 2014) or with media as control. Live counts were used to quantify daily the number of MNs surviving per well and were normalized to day one counts.

Statistics

GraphPad Prism 5.01 (GraphPad Software, La Jolla, CA) was used for statistical analyses. Either one way or two-way repeated ANOVA was conducted followed by Bonferroni post hoc test. All data are graphed as mean \pm SEM.

Results

Connexin 43 Expression is Significantly Elevated in Spinal Cords of the SOD1^{G93A} Mice

To understand if the predominant astrocyte connexin, Cx43, is affected during the course of ALS, we characterized Cx43 expression in SOD1^{G93A} mice temporally and anatomically. We profiled the expression pattern of Cx43 in the spinal cord of SOD1^{G93A} mice at a presymptomatic age (60 days), symptomatic age (90 days) and at endstage (120–140 days) of the disease. We observed that compared to the wild type (WT) mice (Fig. 1A), a temporal increase occurs in the expression of Cx43 in the lumbar spinal cord of SOD1^{G93A} mice (Fig. 1B). Cx43 levels increased significantly to 2.5 fold at endstage in SOD1^{G93A} mice with a minor increase at pre-symptomatic and early symptomatic stages (Fig. 1C). We also observed a significant increase in Cx43 expression in the thoracic and cervical spinal cord at endstage of the SOD1^{G93A} mice compared to WT mice at the same age (Fig. 1D). Immunohistochemical staining for Cx43 in the lumbar spinal cord shows intense labeling of Cx43 (Fig. 1F, F') especially in the gray matter of SOD1^{G93A} mice compared to WT mice. There is co-localization of Cx43 with astrocytes (Fig. 1G, G').

In addition to Cx43, we also examined the other astrocyte connexin, Cx30, in the lumbar spinal cord of SOD1^{G93A} mice (Fig. 2). The protein levels were examined using immunoblotting analysis and no significant difference was detected between lumbar spinal cord of endstage SOD1^{G93A} mice and their WT littermate controls (Fig. 2A, B). However, immunohistochemical staining displays a patchy loss of Cx30 expression (Fig. 2D, D') in the ventral gray matter of SOD1^{G93A} lumbar spinal cord along with marked astrogliosis (Fig. 2C, C') compared to control lumbar spinal cord (Fig. 2E, E').

Human ALS Brain and Spinal Cord Show Increased Expression of Cx43

To establish whether increased levels of Cx43 detected in SOD1^{G93A} spinal cord were reflected in ALS patients, we examined Cx43 expression in human ALS neural tissue and compared them to age-matched control patients (Table I). We quantified gene expression for Cx43 using NanoString analysis in the motor cortex, cervical and lumbar spinal cord. We noted elevated transcript levels of Cx43 in sporadic ALS patients compared to control patients (Fig. 3A–C). When we evaluated the protein expression of Cx43, we observed a dramatic upregulation of Cx43 protein with ~2-fold increase in the motor cortex (Fig. 3A', D) and cervical cord (Fig. 3B', D) and an even more substantial ~8-fold increase of Cx43 expression in lumbar cord (Fig. 3C', D) of ALS patients compared to the control patients. Likewise, the immunohistochemical analysis of the cervical spinal cord revealed a prominent gray matter increase of Cx43 expression in ALS patients compared to control patients (Fig. 3E).

Independent of Neuronal Death, SOD1^{G93A} Astrocytes and Human ALS iPSC-Derived Astrocytes Display Increases in Cx43 Expression

We wanted to assess whether the elevated Cx43 levels observed in SOD1^{G93A} spinal cord and ALS patient tissues could potentially be a consequence of the astrocytic response to neuronal cell death or an endogenous property of ALS astrocytes. To address this, we isolated glial restricted precursor cells (GRPs) as previously reported from the spinal cords of SOD1^{G93A} mice and from transgenic mice over-expressing the wild type SOD1 protein (SOD1^{WT}) (Lepore et al., 2008b). We cultured the GRPs and differentiated them into astrocytes allowing them to reach confluency to enable GJ formation. SOD1^{G93A} astrocytes exhibited an increase in Cx43 and glial fibrillary acidic protein (GFAP) RNA levels (Fig. 4A) and protein levels (Fig. 4B) compared to SOD1^{WT} astrocytes. Furthermore, by culturing astrocytes overexpressing SOD1^{G93A} and comparing them to astrocytes overexpressing SOD1^{WT}, we demonstrate that the increase in Cx43 expression in SOD1^{G93A} astrocytes is not just a function of transgene over-expression but is specific to the mutant form of the SOD1 protein. Since these astrocytes are grown in the absence of neurons, these data also suggest that increase in Cx43 is an inherent property of SOD1^{G93A} astrocytes and not merely related to reactive astrogliosis from neuronal death.

The Cx43 changes observed in human ALS patients prompted us to investigate if, similar to mouse SOD1^{G93A} astrocytes, the increase in Cx43 expression is inherent to human ALS astrocytes. We employed human iPSCs from control patients and ALS patients and differentiated them towards an astrocyte fate (Table II). As reported previously (Haidet-Phillips et al., 2014) and as shown in Fig. 4C, these astrocytes express the appropriate cellular markers and also exhibit membrane localization of Cx43. A confluent layer of astrocytes was cultured and isolated for Cx43 protein analysis. We observed that Cx43 was upregulated ~3 fold in SOD1 ALS patients and a dramatic (~6 fold) increase was noted in patients with C9ORF72 repeat expansion compared to control patient derived astrocytes. Importantly, sporadic ALS iPSC astrocytes (similar to sporadic ALS tissues) also show significantly elevated Cx43 expression in astrocytes with a ~5 fold increase compared to control astrocytes (Fig. 4D). These results imply that astrocytes from ALS patients are intrinsically different in their expression of Cx43 and highly elevated both in familial and

sporadic ALS population, potentially making Cx43 a common mechanism in astrocyte-mediated disease progression.

SOD1^{G93A} Astrocytes Possess Aberrant Cx43 Mediated Functional Properties

To establish whether the increase in Cx43 expression translates to functional changes, we performed several assays relevant to connexin functions. One of the key pathways through which astrocytes communicate involves calcium signaling and the propagation of intracellular calcium waves (Orellana et al., 2012). When astrocytes are mechanically stimulated using a glass micropipette without any chemical activation, this stimulation gives rise to calcium waves. These waves are mediated at least in part by Cx43. We conducted live cell imaging on astrocytes as shown in Fig. 5A. Six different regions were measured for intensity of calcium responses from the point of stimulation (represented by the circle E1) to the farthest distance or region (E6) of the calcium response. We noted that the Fura-2 ratios of SOD1^{G93A} astrocytes (red bar, Fig. 5B) were significantly higher than SOD1^{WT} astrocytes (black bar, Fig. 5B) indicative of higher calcium response seen at the point of stimulation as well as at increasing distances away from the point of stimulation. Thus mechanical stimulation of SOD1^{G93A} astrocytes leads to enhanced calcium intracellular response, which is in part mediated through Cx43 GJs and hemichannels.

ATP stimulation of astrocytes activates P2X receptors and increases calcium signals that are further transmitted through GJs (Hamilton et al., 2008). Increased calcium dynamics in SOD1^{G93A} astrocytes has been previously reported when stimulated using ATP. This increase in intracellular calcium levels was noted to be an increased load of ER calcium in these astrocytes (Kawamata et al., 2014). We used this ATP stimulation paradigm and saw a significant increase in intracellular calcium levels in SOD1^{G93A} astrocytes compared to SOD1^{WT} astrocytes (Fig. 5C, D). However, when we incubated the astrocytes with a Cx43-specific peptide GAP26 (Desplantez et al., 2012) prior to the stimulation, calcium levels of both SOD1^{WT} and SOD1^{G93A} astrocytes were decreased. These data imply that Cx43 GJs and hemichannels contribute to the increased intracellular calcium levels observed in the SOD1^{G93A} astrocytes and that altered Cx43 levels lead to aberrant cellular calcium signaling.

We next tested if increased Cx43 expression changes Cx43-mediated GJ coupling and hemichannel mediated uptake/release, which in turn can affect the homeostatic function of astrocytes. For testing GJ coupling in astrocytes, we conducted a scrape-loading assay on confluent astrocyte layers loaded with 5 μ M of Lucifer yellow (LY) dye (Fig. 6A–C). After performing the scrape assay, the distance of LY dye diffusion from the scrape point was measured. SOD1^{G93A} astrocytes showed ~3-fold increase in LY dye diffusion when compared with SOD1^{WT} astrocytes (Fig. 6B, D). When the astrocytes were incubated with the Cx43 blocker GAP26, a decrease in diffusion of LY dye was noted, although the dye was still taken up by the astrocytes proximal to the scratch area (Fig. 6C) in both SOD1^{WT} and SOD1^{G93A} astrocytes. GAP26 reduced LY dye spreading in SOD1^{WT} astrocytes by 85%, while a 96.7% reduction was observed in SOD1^{G93A} astrocytes. This implies an increase in GJ coupling occurs in the SOD1^{G93A} astrocyte network that is primarily mediated through Cx43.

The hemichannel activity of astrocytes is increased under inflammatory conditions. One example is that the treatment of astrocytes with amyloid beta for 72 hours increased their hemichannel activity, mediated through Cx43 hemichannels (Orellana et al., 2011b). Therefore, we tested if hemichannel activity is altered between SOD1^{G93A} astrocytes and SOD1^{WT} astrocytes. Ethidium bromide (EtBr) uptake was used as a measure of hemichannel activity. We observed that astrocytes from SOD1^{G93A} mice had increased EtBr uptake compared to astrocytes from SOD1^{WT} mice (Fig. 7A, B, G). Further, when astrocytes were exposed to the pro-inflammatory cytokines IL-1 β (10 μ M) and TNF- α (10 μ M) for 24 hrs., a modest increase in EtBr uptake was observed in SOD1^{WT} astrocytes (Fig. 7C, G). However, SOD1^{G93A} astrocytes showed a substantial ~3-fold increase in EtBr uptake compared to SOD1^{WT} astrocytes (Fig. 7D, G). Interestingly, when astrocytes treated with the cytokines were incubated with 200 μ M of GAP26 along with EtBr, the hemichannel uptake in SOD1^{G93A} astrocytes returned to baseline (Fig. 7F, G), indicating that the increased hemichannel activity in SOD1^{G93A} astrocytes is mediated via Cx43 hemichannels. SOD1^{WT} astrocytes did not show much effect upon cytokine stimulation or the use of GAP26 (Fig. 7C, E, G), which could suggest that a more potent inflammatory stimulus may be needed to observe the same effect as seen with SOD1^{G93A} astrocytes. Collectively, these results suggest that astrocytes isolated from SOD1^{G93A} mice not only have increased Cx43 expression compared to control astrocytes but also have increase in GJ and hemichannel functions independent of neuronal input and/or death.

Blockade of Cx43 in SOD1^{G93A} Astrocytes Is Neuroprotective to Motor Neurons In Vitro

To examine whether changes in Cx43 expression and function could contribute, at least in part, to motor neuron vulnerability, we utilized an astrocyte-motor neuron co-culture system. We tested if blocking Cx43 GJs and/or hemichannels is protective to the previously reported SOD1^{G93A} astrocyte mediated toxicity on motor neurons (Haidet-Phillips et al., 2011). We cultured astrocytes derived from SOD1^{G93A} and SOD1^{WT} mice and then co-cultured them with mouse embryonic stem cell derived MNs that express green fluorescent protein (GFP) under the control of the motor neuron-specific HB9 promoter. We observed that FACS sorted GFP⁺ MNs cultured with SOD1^{G93A} astrocytes (Fig. 8B, B') degenerated more rapidly compared to MNs on SOD1^{WT} astrocytes (Fig. 8A, A'). However, when MNs plated on SOD1^{G93A} astrocytes were treated with the Cx43 blocker GAP26, MNs survived significantly better compared to untreated MNs on SOD1^{G93A} astrocytes (Fig. 8C, C'). GAP26 acts on both Cx43 GJs as well as hemichannels (Desplantez et al., 2012). To further elucidate the role of Cx43 hemichannels on MN survival, we employed a Cx43 hemichannel-specific blocker GAP19. We observed that MNs plated on SOD1^{G93A} astrocytes and treated with GAP19 conferred significant neuroprotection (Fig. 8D, D', E), similar to MNs treated with GAP26. Treatment of SOD1^{G93A} astrocytes with Cx43 blockers results in survival of twice as many motor neurons compared to untreated motor neurons (Fig. 8E). These results imply that blocking abnormal Cx43 mediated functions in SOD1^{G93A} astrocytes *in vitro* is neuroprotective to MNs. As the Cx43 hemichannel blocker (GAP19) provided comparable (and not additive) neuroprotection to the Cx43 GJ and hemichannel blocker (GAP26), these data indicate that hemichannels primarily contribute to Cx43 mediated toxicity *in vitro*.

Discussion

Astrocytes are implicated in the progression of ALS following disease onset (Yamanaka et al., 2008), making them an attractive target for manipulation to potentially slow disease progression in ALS. While previous studies have demonstrated the non-cell autonomous role of astrocytes in MN death, emerging studies are now focusing on the molecular mechanisms underlying astrocyte-mediated toxicity to MNs. We examined the role of Cx43, a key player in CNS homeostasis in the context of ALS and observed how Cx43 is altered in expression and function, eventually contributing to toxicity of motor neurons in ALS. In addition to holding important physiological functions outside the CNS (Dbouk et al., 2009), Cx43 is a major astrocyte GJ protein in the CNS (Cotrina et al., 2001).

Our data show that Cx43 expression is upregulated in all three segments of the SOD1^{G93A} spinal cord at endstage. Interestingly, levels of Cx43 increase in a temporal manner, as reported previously by Cui *et.al* (Cui et al., 2014). It is possible that the increase in Cx43 is a compensatory effect due to the patchy loss of Cx30 in the ventral gray matter of SOD1^{G93A} spinal cord. Another possible reason for the early temporal increase in Cx43 expression could be due to the reactive state of astrocytes in SOD1^{G93A} mouse or a feature of astrocytes harboring the SOD1^{G93A} mutation. Reactive astrogliosis is a phenomenon observed in several disorders of the CNS such as ALS (Howland et al., 2002), spinal cord injury (Huang et al., 2012), Alzheimer's disease (Koulakoff et al., 2012) and even normal process of aging (Middeldorp and Hol 2011). In ALS, reduction in astrogliosis by the inhibition of astrocyte proliferation did not affect the disease phenotype (Lepore et al., 2008a). These studies have raised the question as to how the upregulation of astrocytic proteins affects astrocyte function and whether their upregulation results in a neuroprotective effect, a bystander effect or perhaps contribute to neurodegeneration.

To explore whether the increase in Cx43 is an endogenous phenomenon to SOD1^{G93A} astrocytes or whether this increase is a secondary effect related to motor neuron loss, we utilized GRPs from SOD1^{G93A} mice to differentiate into astrocytes. We found that even in the absence of neurons, SOD1^{G93A} astrocytes show significant increase in Cx43 levels compared with astrocytes over-expressing SOD1^{WT}, indicating this phenotype is not facilitated due to mere over-expression of the SOD1 protein but is specific to the mutation.

In parallel to mouse spinal cord astrocytes, when we differentiated astrocytes from human iPSCs, we examined a significant increase in Cx43 expression in astrocytes from patients with SOD1 mutation, C9ORF72 repeat expansion and sporadic ALS patients compared to astrocytes from control patients. These data suggest that the increase in Cx43 is an inherent property of ALS astrocytes. On inspecting postmortem tissues from sporadic ALS patients, we similarly observed that Cx43 expression increased in comparison to control patients. Together these data demonstrate that increase in Cx43 expression is a common feature observed in iPSC-derived astrocytes and neural tissues from familial and sporadic ALS patients. This suggests that, at least for connexin biology, murine modeling may offer some parallels to human disease.

We further explored the connexin properties—calcium signaling, gap junctional coupling and hemichannel activity as a functional readout out of altered connexin 43 levels in SOD1^{G93A} astrocytes. We demonstrated that SOD1^{G93A} astrocytes displayed increased intracellular calcium responses upon ATP stimulation and upon mechanical stimulation compared to SOD1^{WT} astrocytes. Previous works suggest abnormal calcium dynamics in ALS astrocytes (Milosevic et al., 2016; Fritz et al., 2013; Cassina et al., 2008; Kawamata and Manfredi, 2010) contributed by factors such as excess intracellular calcium release from ER stores (Kawamata et al., 2014) or mGLUR5 mediated increase in intracellular calcium contribution (Rossi et al., 2008). GJ and hemichannel-mediated calcium waves form a key signaling pathway for astrocyte networks (De Bock et al., 2012) and here we show that Cx43 also contributes to the increased calcium responses observed in SOD1^{G93A} astrocytes. We further examined that increase in Cx43 leads to enhanced GJ coupling in SOD1^{G93A} astrocytes compared to control astrocytes. Additionally, as seen in models of Alzheimer's disease, HIV infected astrocytes and bacterial meningitis (Kielian, 2008), we observed an increase in Cx43 hemichannel activity in SOD1^{G93A} astrocytes, which intensified upon cytokine stimulation. We illustrated this increase in hemichannel activity is mediated by Cx43, as the use of a Cx43 blocker GAP26 returned the hemichannel activity to baseline in SOD1^{G93A} astrocytes. In other models of neuroinflammation such as bacterial meningitis (Kielian, 2008) and Niemann-Pick type C (NPC) disease (Saez et al., 2013), increased hemichannel activity is accompanied by a decrease in the gap junction coupling. However, in our current ALS model, we observed an increase in both gap junction coupling and hemichannel activity. This difference could be potentially due to the overall increase in total Cx43 protein levels seen in our model compared to other models, which leads to increased recruitment of Cx43 and enhanced associated functions. This enhanced gap junction function could also be a compensatory effect for loss of glutamate transporter GLT-1 (Unger et al., 2012) or potentially due to loss of Cx30 and its associated functions.

Abnormal Cx43 properties in other neurodegenerative diseases are known to affect the health and survival of neurons (Kielian, 2008). In light of this, we examined if changes in Cx43 affects the survival of motor neurons using a co-culture system. We observed loss of motor neurons when cultured with SOD1^{G93A} astrocytes compared to SOD1^{WT} astrocytes over time. However, addition of a Cx43 blocker GAP26 (that acts on both gap junctions and hemichannels) to SOD1^{G93A} astrocytes salvaged the loss of motor neurons resulting in neuroprotection. To understand if this neuroprotection is mediated through Cx43 GJs or hemichannels, we further tested the effects of a Cx43 hemichannel specific blocker GAP19 on motor neurons and observed a neuroprotective effect similar to GAP26 treatment. These results imply that the neuroprotection conferred by blocking Cx43 is primarily due to an increase in hemichannel function. Similar protective effects of blocking Cx43 have been described in models of hypoxia, Alzheimer's, HIV, ischemia, etc. (Chew et al., 2010). As discussed above, increased Cx43 function eventually impacts and contributes to motor neuron death in ALS model as seen in other neurodegenerative models. Calcium signaling is an important second messenger, but excessive calcium signaling can be excitotoxic, propagating and amplifying the signals along astrocyte networks. The increased gap junction communication can be a potential mechanism for disease spreading in ALS where toxic signals are propagated across astrocyte networks as seen in ischemic models (Lin et al.,

1998). For future studies, it will be important to test if blocking gap junction *in vivo* can slow disease propagation in ALS animal models.

Microglia release proinflammatory cytokines such as IL-1 β and TNF- α that enhance Cx43 hemichannel function in astrocytes, releasing glutamate and ATP that further contributes to neuronal death (Abudara et al., 2015; Froger et al., 2010). In ALS, microglia have been shown to induce motor neuron cell death although the relationship between microglia and astrocyte connexins in the context of ALS have not been extensively explored.

Local hemichannel activity can release second messengers such as glutamate, ATP, calcium, etc. There is evidence that extracellular ATP leads to over-activation of P2X7 receptors in SOD1^{G93A} astrocytes that results in the eventual demise of motor neurons in a co-culture system (Gandelman et al., 2010; Orellana et al., 2011a).

Here we established that the homeostatic function of Cx43 in astrocytes is compromised, resulting in an astrocyte mediated toxic effect on motor neurons in ALS. Future studies that modulate Cx43 expression, and therefore function *in vivo* will help tease-out the relationship of astrocyte-specific Cx43 to the regulation of other CNS connexins as well as elucidate pathological and phenotypic alterations to ALS disease progression. As astrocytes contribute to disease progression in ALS, the connexin-mediated changes that we have observed warrant further investigation as to whether modulating Cx43-mediated functions may be beneficial in ALS management and disease progression following a diagnosis.

Acknowledgments

Grant sponsor: Maryland Stem Cell Research Fund postdoctoral fellowship, Robert Packard Center for ALS Research; Grant number: NIH R21NS093244

The authors thank Dr. Kevin Eggen and Dr. Thomas Jessell for the HB9-GFP embryonic stem cells. They thank Dr. Rebecca Marrero for her assistance in some of the experiments. They also thank Department of Veterans Affairs, VA Biospository for generously providing us with human ALS samples.

References

- Abudara V, Bechberger J, Freitas-Andrade M, De Bock M, Wang N, Bultynck G, Naus CC, Leybaert L, Giaume C. The connexin43 mimetic peptide Gap19 inhibits hemichannels without altering gap junctional communication in astrocytes. *Front Cell Neurosci.* 2014; 8:306. [PubMed: 25374505]
- Abudara V, Roux L, Dallerac G, Matias I, Dulong J, Mothet JP, Rouach N, Giaume C. Activated microglia impairs neuroglial interaction by opening Cx43 hemichannels in hippocampal astrocytes. *Glia.* 2015; 63:795–811. [PubMed: 25643695]
- Avendano BC, Montero TD, Chavez CE, von Bernhardt R, Orellana JA. Prenatal exposure to inflammatory conditions increases Cx43 and Panx1 unopposed channel opening and activation of astrocytes in the offspring effect on neuronal survival. *Glia.* 2015; 63:2058–2072.
- Bennett MV, Contreras JE, Bukauskas FF, Saez JC. New roles for astrocytes: Gap junction hemichannels have something to communicate. *Trends Neurosci.* 2003; 26:610–617. [PubMed: 14585601]
- Bruijn LI, Becher MW, Lee MK, Anderson KL, Jenkins NA, Copeland NG, Sisodia SS, Rothstein JD, Borchelt DR, Price DL, et al. ALS-linked SOD1 mutant G85R mediates damage to astrocytes and promotes rapidly progressive disease with SOD1-containing inclusions. *Neuron.* 1997; 18:327–338. [PubMed: 9052802]
- Cassina P, Cassina A, Pehar M, Castellanos R, Gandelman M, de Leon A, Robinson KM, Mason RP, Beckman JS, Barbeito L, Almad Akshata A, Doreswamy Arpitha, Gross Sarah K, Richard Jean-

- Philippe, Huo Yuqing, Haughey Norman, Maragakis Nicholas J. Mitochondrial dysfunction in SOD1G93A-bearing astrocytes promotes motor neuron degeneration: Prevention by mitochondrial-targeted antioxidants. *J Neurosci*. 2008; 28:4115–4122. [PubMed: 18417691]
- Chen MJ, Kress B, Han X, Moll K, Peng W, Ji RR, Nedergaard M. Astrocytic CX43 hemichannels and gap junctions play a crucial role in development of chronic neuropathic pain following spinal cord injury. *Glia*. 2012; 60:1660–1670. [PubMed: 22951907]
- Chew SS, Johnson CS, Green CR, Danesh-Meyer HV. Role of connexin43 in central nervous system injury. *Exp Neurol*. 2010; 225:250–261. [PubMed: 20655909]
- Clement AM, Nguyen MD, Roberts EA, Garcia ML, Boillee S, Rule M, McMahon AP, Doucette W, Siwek D, Ferrante RJ, et al. Wild-type non-neuronal cells extend survival of SOD1 mutant motor neurons in ALS mice. *Science*. 2003; 302:113–117. [PubMed: 14526083]
- Cotrina ML, Gao Q, Lin JH, Nedergaard M. Expression and function of astrocytic gap junctions in aging. *Brain Res*. 2001; 901:55–61. [PubMed: 11368950]
- Cui Y, Masaki K, Yamasaki R, Imamura S, Suzuki SO, Hayashi S, Sato S, Nagara Y, Kawamura MF, Kira J. Extensive dysregulations of oligodendrocytic and astrocytic connexins are associated with disease progression in an amyotrophic lateral sclerosis mouse model. *J Neuroinflammation*. 2014; 11:42. [PubMed: 24597481]
- Dbouk HA, Mroue RM, El-Sabban ME, Talhouk RS. Connexins: A myriad of functions extending beyond assembly of gap junction channels. *Cell Commun Signal*. 2009; 7:4. [PubMed: 19284610]
- De Bock M, Wang N, Bol M, Decrock E, Ponsaerts R, Bultynck G, Dupont G, Leybaert L. Connexin 43 hemichannels contribute to cytoplasmic Ca²⁺ oscillations by providing a bimodal Ca²⁺-dependent Ca²⁺ entry pathway. *J Biol Chem*. 2012; 287:12250–12266. [PubMed: 22351781]
- Desplantez T, Verma V, Leybaert L, Evans WH, Weingart R. Gap26, a connexin mimetic peptide, inhibits currents carried by connexin43 hemichannels and gap junction channels. *Pharmacol Res*. 2012; 65:546–552. [PubMed: 22406236]
- Di Giorgio FP, Carrasco MA, Siao MC, Maniatis T, Eggan K. Non-cell autonomous effect of glia on motor neurons in an embryonic stem cell-based ALS model. *Nat Neurosci*. 2007; 10:608–614. [PubMed: 17435754]
- Diaz-Amarilla P, Olivera-Bravo S, Trias E, Cragnolini A, Martinez-Palma L, Cassina P, Beckman J, Barbeito L. Phenotypically aberrant astrocytes that promote motoneuron damage in a model of inherited amyotrophic lateral sclerosis. *Proc Natl Acad Sci USA*. 2011; 108:18126–18131. [PubMed: 22010221]
- Fritz E, Izaurieta P, Weiss A, Mir FR, Rojas P, Gonzalez D, Rojas F, Brown RHJ, Madrid R, van Zundert B. Mutant SOD1-expressing astrocytes release toxic factors that trigger motoneuron death by inducing hyperexcitability. *J Neurophysiol*. 2013; 109:2803–2814. [PubMed: 23486205]
- Froger N, Orellana JA, Calvo CF, Amigou E, Kozoriz MG, Naus CC, Saez JC, Giaume C. Inhibition of cytokine-induced connexin43 hemichannel activity in astrocytes is neuroprotective. *Mol Cell Neurosci*. 2010; 45:37–46. [PubMed: 20684043]
- Gandelman M, Peluffo H, Beckman JS, Cassina P, Barbeito L. Extracellular ATP and the P2X7 receptor in astrocyte-mediated motor neuron death: Implications for amyotrophic lateral sclerosis. *J Neuroinflammation*. 2010; 7:33. [PubMed: 20534165]
- Giaume C, Liu X. From a glial syncytium to a more restricted and specific glial networking. *J Physiol Paris*. 2012; 106:34–39. [PubMed: 21979115]
- Giaume C, Orellana JA, Abudara V, Saez JC. Connexin-based channels in astrocytes: how to study their properties. *Methods Mol Biol*. 2012; 814:283–303. [PubMed: 22144314]
- Gosejacob D, Dublin P, Bedner P, Huttmann K, Zhang J, Tress O, Willecke K, Pfrieger F, Steinhauser C, Theis M. Role of astroglial connexin30 in hippocampal gap junction coupling. *Glia*. 2011; 59:511–519. [PubMed: 21264956]
- Haidet-Phillips AM, Hester ME, Miranda CJ, Meyer K, Braun L, Frakes A, Song S, Likhite S, Murtha MJ, Foust KD, et al. Astrocytes from familial and sporadic ALS patients are toxic to motor neurons. *Nat Biotechnol*. 2011; 29:824–828. [PubMed: 21832997]
- Haidet-Phillips AM, Roybon L, Gross SK, Tuteja A, Donnelly CJ, Richard JP, Ko M, Sherman A, Eggan K, Henderson CE, et al. Gene profiling of human induced pluripotent stem cell-derived

- astrocyte progenitors following spinal cord engraftment. *Stem Cells Transl Med.* 2014; 3:575–585. [PubMed: 24604284]
- Hamilton N, Vayro S, Kirchhoff F, Verkhatsky A, Robbins J, Gorecki DC, Butt AM. Mechanisms of ATP- and glutamate-mediated calcium signaling in white matter astrocytes. *Glia.* 2008; 56:734–749. [PubMed: 18293404]
- Howland DS, Liu J, She Y, Goad B, Maragakis NJ, Kim B, Erickson J, Kulik J, DeVito L, Psaltis G, et al. Focal loss of the glutamate transporter EAAT2 in a transgenic rat model of SOD1 mutant-mediated amyotrophic lateral sclerosis (ALS). *Proc Natl Acad Sci USA.* 2002; 99:1604–1609. [PubMed: 11818550]
- Huang C, Han X, Li X, Lam E, Peng W, Lou N, Torres A, Yang M, Garre JM, Tian GF, et al. Critical role of connexin 43 in secondary expansion of traumatic spinal cord injury. *J Neurosci.* 2012; 32:3333–3338. [PubMed: 22399755]
- Ilieva H, Polymenidou M, Cleveland DW. Non-cell autonomous toxicity in neurodegenerative disorders: ALS and beyond. *J Cell Biol.* 2009; 187:761–772. [PubMed: 19951898]
- Kawamata H, Manfredi G. Mitochondrial dysfunction and intracellular calcium dysregulation in ALS. *Mech Ageing Dev.* 2010; 131:517–526. [PubMed: 20493207]
- Kawamata H, Ng SK, Diaz N, Burstein S, Morel L, Osgood A, Sider B, Higashimori H, Haydon PG, Manfredi G, et al. Abnormal intracellular calcium signaling and SNARE-dependent exocytosis contributes to SOD1G93A astrocyte-mediated toxicity in amyotrophic lateral sclerosis. *J Neurosci.* 2014; 34:2331–2348. [PubMed: 24501372]
- Keller AF, Gravel M, Kriz J. Treatment with minocycline after disease onset alters astrocyte reactivity and increases microgliosis in SOD1 mutant mice. *Exp Neurol.* 2011; 228:69–79. [PubMed: 21168408]
- Kerr NM, Johnson CS, Zhang J, Eady EK, Green CR, Danesh-Meyer HV. High pressure-induced retinal ischaemia reperfusion causes upregulation of gap junction protein connexin43 prior to retinal ganglion cell loss. *Exp Neurol.* 2012; 234:144–152. [PubMed: 22226601]
- Kielian T. Glial connexins and gap junctions in CNS inflammation and disease. *J Neurochem.* 2008; 106:1000–1016. [PubMed: 18410504]
- Konietzko U, Muller CM. Astrocytic dye coupling in rat hippocampus: Topography, developmental onset, and modulation by protein kinase C. *Hippocampus.* 1994; 4:297–306. [PubMed: 7842053]
- Koulakoff A, Mei X, Orellana JA, Saez JC, Giaume C. Glial connexin expression and function in the context of Alzheimer's disease. *Biochim Biophys Acta.* 2012; 1818:2048–2057. [PubMed: 22008509]
- Lepore AC, Dejea C, Carmen J, Rauck B, Kerr DA, Sofroniew MV, Maragakis NJ. Selective ablation of proliferating astrocytes does not affect disease outcome in either acute or chronic models of motor neuron degeneration. *Exp Neurol.* 2008a; 211:423–432. [PubMed: 18410928]
- Lepore AC, Haenggeli C, Gasmi M, Bishop KM, Bartus RT, Maragakis NJ, Rothstein JD. Intraparenchymal spinal cord delivery of adeno-associated virus IGF-1 is protective in the SOD1G93A model of ALS. *Brain Res.* 2007; 1185:256–265. [PubMed: 17963733]
- Lepore AC, Rauck B, Dejea C, Pardo AC, Rao MS, Rothstein JD, Maragakis NJ. Focal transplantation-based astrocyte replacement is neuroprotective in a model of motor neuron disease. *Nat Neurosci.* 2008b; 11:1294–1301. [PubMed: 18931666]
- Lin JH, Weigel H, Cotrina ML, Liu S, Bueno E, Hansen AJ, Hansen TW, Goldman S, Nedergaard M. Gap-junction-mediated propagation and amplification of cell injury. *Nat Neurosci.* 1998; 1:494–500. [PubMed: 10196547]
- Marchetto MC, Muotri AR, Mu Y, Smith AM, Cezar GG, Gage FH. Non-cell-autonomous effect of human SOD1 G37R astrocytes on motor neurons derived from human embryonic stem cells. *Cell Stem Cell.* 2008; 3:649–657. [PubMed: 19041781]
- Meyer K, Ferraiuolo L, Miranda CJ, Likhite S, McElroy S, Rensch S, Ditsworth D, Lagier-Tourenne C, Smith RA, Ravits J, et al. Direct conversion of patient fibroblasts demonstrates non-cell autonomous toxicity of astrocytes to motor neurons in familial and sporadic ALS. *Proc Natl Acad Sci USA.* 2014; 111:829–832. [PubMed: 24379375]
- Middeldorp J, Hol EM. GFAP in health and disease. *Prog Neurobiol.* 2011; 93:421–443. [PubMed: 21219963]

- Milosevic M, Bataveljic D, Nikolic L, Bijelic D, Andjus P. The effect of amyotrophic lateral sclerosis-linked exogenous SOD1-G93A on electrophysiological properties and intracellular calcium in cultured rat astrocytes. *Amyotroph Lateral Scler Frontotemporal Degener.* 2016; 19:1–9.
- Nagai M, Re DB, Nagata T, Chalazonitis A, Jessell TM, Wichterle H, Przedborski S. Astrocytes expressing ALS-linked mutated SOD1 release factors selectively toxic to motor neurons. *Nat Neurosci.* 2007; 10:615–622. [PubMed: 17435755]
- Nagy JI, Li W, Hertzberg EL, Marotta CA. Elevated connexin43 immunoreactivity at sites of amyloid plaques in Alzheimer's disease. *Brain Res.* 1996; 717:173–178. [PubMed: 8738268]
- Orellana JA, Froger N, Ezan P, Jiang JX, Bennett MV, Naus CC, Giaume C, Saez JC. ATP and glutamate released via astroglial connexin 43 hemichannels mediate neuronal death through activation of pannexin 1 hemichannels. *J Neurochem.* 2011a; 118:826–840. [PubMed: 21294731]
- Orellana JA, Saez PJ, Shoji KF, Schalper KA, Palacios-Prado N, Velarde V, Giaume C, Bennett MV, Saez JC. Modulation of brain hemichannels and gap junction channels by pro-inflammatory agents and their possible role in neurodegeneration. *Antioxid Redox Signal.* 2009; 11:369–399. [PubMed: 18816186]
- Orellana JA, Sanchez HA, Schalper KA, Figueroa V, Saez JC. Regulation of intercellular calcium signaling through calcium interactions with connexin-based channels. *Adv Exp Med Biol.* 2012; 740:777–794. [PubMed: 22453969]
- Orellana JA, Shoji KF, Abudara V, Ezan P, Amigou E, Saez PJ, Jiang JX, Naus CC, Saez JC, Giaume C. Amyloid beta-induced death in neurons involves glial and neuronal hemichannels. *J Neurosci.* 2011b; 31:4962–4977. [PubMed: 21451035]
- Papadeas ST, Kraig SE, O'Banion C, Lepore AC, Maragakis NJ. Astrocytes carrying the superoxide dismutase 1 (SOD1G93A) mutation induce wild-type motor neuron degeneration in vivo. *Proc Natl Acad Sci USA.* 2011; 108:17803–17808. [PubMed: 21969586]
- Rash JE, Yasumura T, Davidson KG, Furman CS, Dudek FE, Nagy JI. Identification of cells expressing Cx43, Cx30, Cx26, Cx32 and Cx36 in gap junctions of rat brain and spinal cord. *Cell Commun Adhes.* 2001; 8:315–320. [PubMed: 12064610]
- Re DB, Le Verche V, Yu C, Amoroso MW, Politi KA, Phani S, Ikiz B, Hoffmann L, Koolen M, Nagata T, et al. Necroptosis drives motor neuron death in models of both sporadic and familial ALS. *Neuron.* 2014; 81:1001–1008. [PubMed: 24508385]
- Robberecht W, Philips T. The changing scene of amyotrophic lateral sclerosis. *Nat Rev Neurosci.* 2013; 14:248–264. [PubMed: 23463272]
- Rocheffort N, Quenech' du N, Ezan P, Giaume C, Milleret C. Postnatal development of GFAP, connexin43 and connexin30 in cat visual cortex. *Brain Res Dev Brain Res.* 2005; 160:252–264. [PubMed: 16297988]
- Rossi D, Brambilla L, Valori CF, Roncoroni C, Crugnola A, Yokota T, Bredesen DE, Volterra A. Focal degeneration of astrocytes in amyotrophic lateral sclerosis. *Cell Death Differ.* 2008; 15:1691–1700. [PubMed: 18617894]
- Rovegno M, Soto PA, Saez PJ, Naus CC, Saez JC, von Bernhardi R. Connexin43 hemichannels mediate secondary cellular damage spread from the trauma zone to distal zones in astrocyte monolayers. *Glia.* 2015; 63:1185–1199. [PubMed: 25731866]
- Saez PJ, Orellana JA, Vega-Riveros N, Figueroa VA, Hernandez DE, Castro JF, Klein AD, Jiang JX, Zanlungo S, Saez JC. Disruption in connexin-based communication is associated with intracellular Ca(2)(+) signal alterations in astrocytes from Niemann-Pick type C mice. *PLoS One.* 2013; 8:e71361. [PubMed: 23977027]
- Sun L, Gao J, Zhao M, Cui J, Li Y, Yang X, Jing X, Wu Z. A novel cognitive impairment mechanism that astrocytic p-connexin 43 promotes neuronal autophagy via activation of P2X7R and down-regulation of GLT-1 expression in the hippocampus following traumatic brain injury in rats. *Behav Brain Res.* 2015; 291:315–324. [PubMed: 26031379]
- Unger T, Bette S, Zhang J, Theis M, Engele J. Connexin-deficiency affects expression levels of glial glutamate transporters within the cerebrum. *Neurosci Lett.* 2012; 506:12–16. [PubMed: 22037505]
- Wichterle H, Lieberam I, Porter JA, Jessell TM. Directed differentiation of embryonic stem cells into motor neurons. *Cell.* 2002; 110:385–397. [PubMed: 12176325]

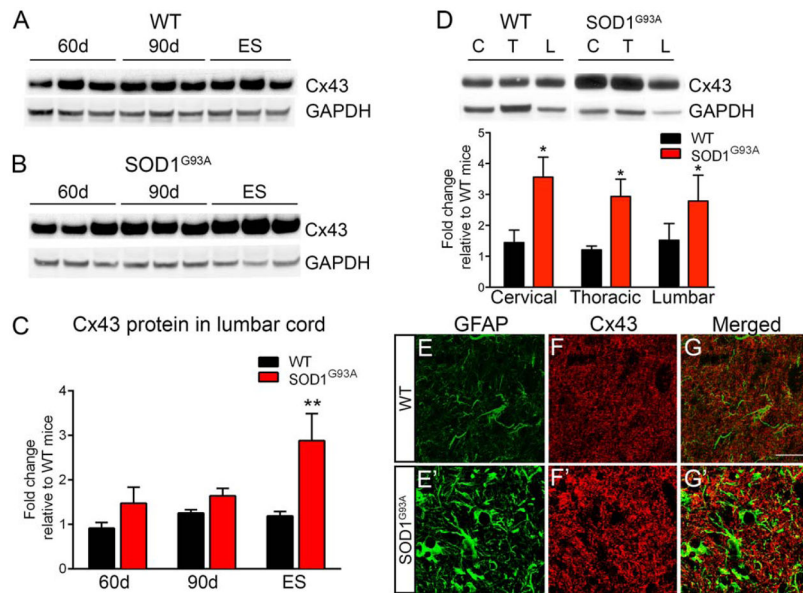
Yamanaka K, Chun SJ, Boillee S, Fujimori-Tonou N, Yamashita H, Gutmann DH, Takahashi R, Misawa H, Cleveland DW. Astrocytes as determinants of disease progression in inherited amyotrophic lateral sclerosis. *Nat Neurosci.* 2008; 11:251–253. [PubMed: 18246065]

Author Manuscript

Author Manuscript

Author Manuscript

Author Manuscript

**FIGURE 1.**

Cx43 levels are significantly increased in the spinal cord of SOD1^{G93A} mice. (A) The protein level of Cx43 and GAPDH from lumbar spinal cord of control littermates at 60 days, 90 days and 120 days was examined. (B) Cx43 levels were elevated in the lumbar cord of SOD1^{G93A} mice compared to control littermate. (C) Cx43 expression was normalized to GAPDH and a significant increase was noted in SOD1^{G93A} mice at endstage compared to control mice, with modest increases at 60 d and 90d. Data is presented as \pm SEM with $n=5$ mice per group per time point. ** $p < 0.01$ by ANOVA with Bonferroni post-hoc analysis. (D) Cx43 expression was also evaluated in the cervical, thoracic, and lumbar spinal cord segments of SOD1^{G93A} and littermate control mice. A 2–3 fold increase was observed in all the segments at end stage of the SOD1^{G93A} mice compared to the control mice sacrificed at similar age. Data is represented as \pm SEM with $n=5$ mice per condition, per genotype and $p < 0.05$ by ANOVA with Bonferroni analysis. Localization of Cx43 in lumbar gray matter of WT control (F) and SOD1^{G93A} mice (F') was observed in astrocytes labeled intensely with GFAP in SOD1^{G93A} mice (E') compared to control mice (E) as shown in the merged images (G, G'). Scale bar =20 μ m.

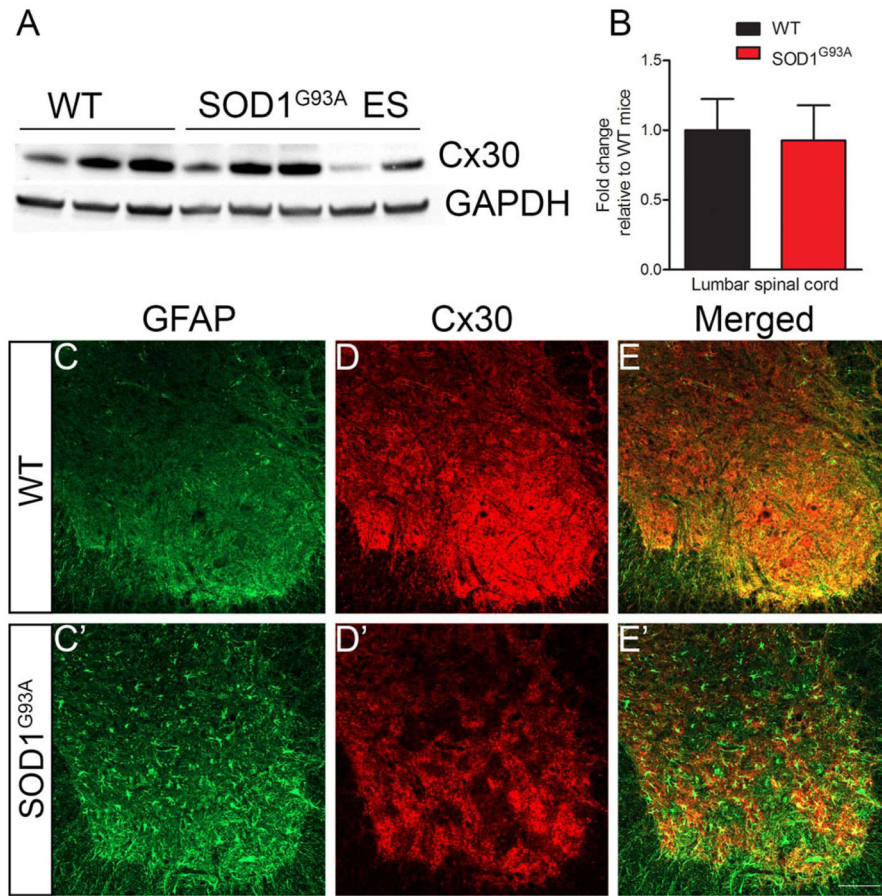


FIGURE 2. Focal loss of Cx30 in the ventral gray matter of SOD1^{G93A} mice. (A–B) Protein expression of Cx30 was examined in the end-stage tissue from lumbar spinal cord of SOD1^{G93A} mice and WT control littermate at the same time point. Cx30 was normalized to GAPDH and no significant changes were observed between WT and SOD1^{G93A} mice (n =3–5 mice/group). (C–E) Immunohistochemical analysis shows increased astroglia in SOD1^{G93A} ventral gray matter (C') compared to control gray matter (C). Interestingly, focal loss of Cx30 was noted in the lumbar gray matter of SOD1^{G93A} mice (D', E') at endstage compared to uniform Cx30 expression in the gray matter of control mice (D, E). n =5 mice/group, scale bar= 100 μ m.

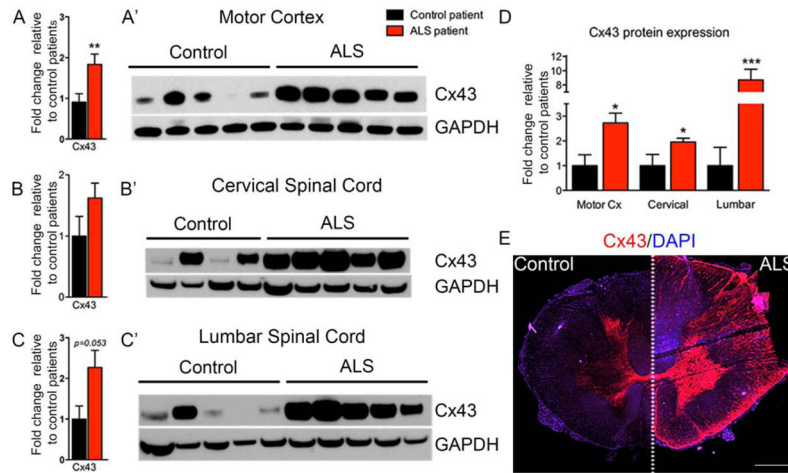
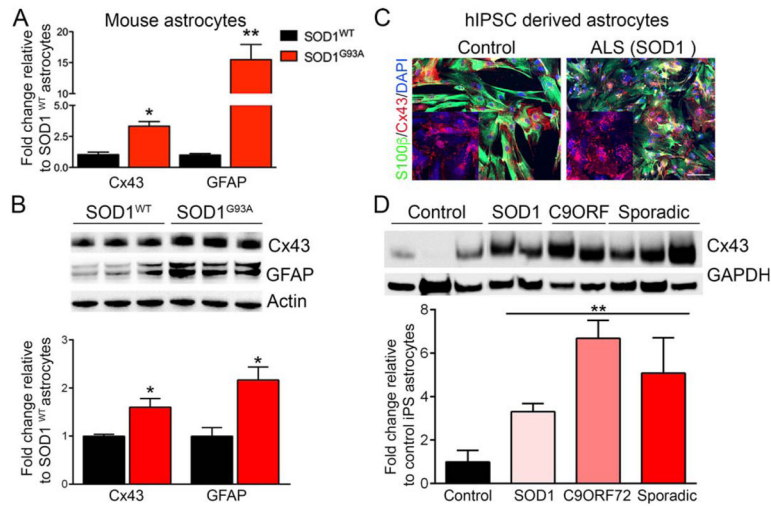
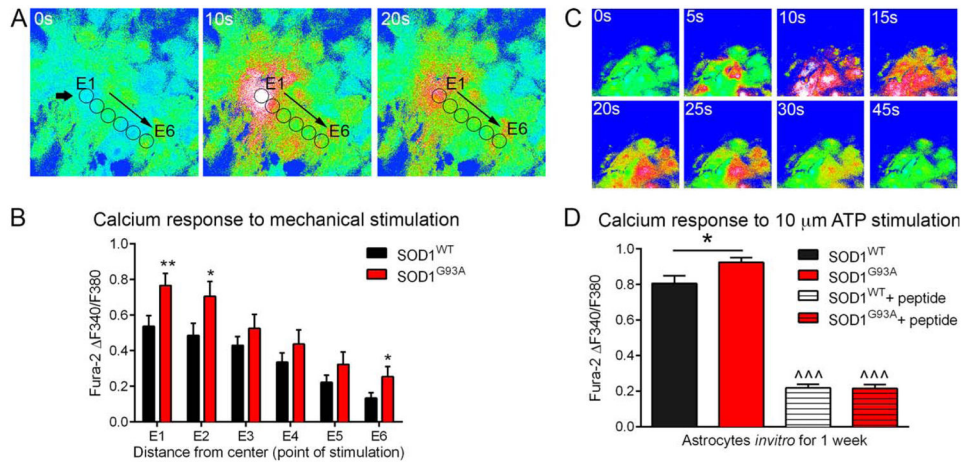


FIGURE 3.

Human post-mortem tissues from ALS patients have elevated Cx43 expression. (A–C) NanoString analysis of motor cortex, cervical and lumbar spinal cord from control and sporadic ALS patients show increased Cx43 gene expression in ALS patients. Data is presented as \pm SEM with $n = 5$ patients per group, $**p < 0.01$ by t-test. The protein level of Cx43 was significantly greater in motor cortex (A'), cervical spinal cord (B'), and lumbar spinal cord (C') of sporadic ALS patients compared to control patients. (D) The protein level of Cx43 that was normalized to GAPDH shows a ~ 2.5 -fold increase in motor cortex of ALS patients, a 2-fold increase in cervical spinal cord and a ~ 8 fold increase in the lumbar spinal cord compared to control patients. Data is presented as \pm SEM with $n = 5$ patients per group per tissue. $*p < 0.05$, $**p < 0.01$, $***p < 0.001$ by ANOVA with Bonferroni post-hoc analysis. (E) Cx43 increase was localized prominently to the gray matter of ALS cervical cord (right) compared to control cervical cord (left). Scale bar = $80\mu\text{m}$.

**FIGURE 4.**

Cx43 expression is inherently elevated in mouse SOD1^{G93A} astrocytes and ALS human iPSC-derived astrocytes. (A) Using qPCR analysis, a significant increase in Cx43 and GFAP levels was detected in SOD1^{G93A} astrocytes compared to SOD1^{WT} astrocytes, which was normalized with 18s RNA. (B) Similarly, increased protein levels of Cx43 and GFAP were detected in SOD1^{G93A} astrocytes compared with SOD1^{WT} astrocytes in vitro, which was normalized to the loading control actin. Data is presented as \pm SEM, n =3 wells per condition. *p < 0.05, **p < 0.01 by ANOVA with Bonferroni analysis. (C) Human iPSC cells from control and ALS patients were differentiated into astrocytes and stained with the astrocyte marker S100 β along with Cx43. Scale bar =100 μ m (D) The iPSC-derived astrocytes from control (n =3) and ALS patients (n =6) were probed for Cx43 levels and was normalized to the loading control GAPDH. Data is presented as \pm SEM for control lines and each of the ALS mutations are plotted individually showing higher Cx43 levels in SOD1^{A4V}, C9ORF72 and sporadic patient lines **p < 0.01.

**FIGURE 5.**

Increased Cx43 expression in SOD1^{G93A} astrocytes mediates increased calcium responses through mechanical and ATP stimulation. (A) Mechanical stimulation of a single astrocyte with a glass micropipette at point of stimulation (black arrow, E1) generated calcium waves. (B) Quantification of calcium response in cells loaded with Fura-2 at 340 nm and 380 nm depicted increased calcium response of SOD1^{G93A} astrocytes (red bar) compared with SOD1^{WT} astrocytes (black bar) from point of stimulation E1 and different points away from point of stimulation. Data is presented as \pm SEM with $n=9-10$ coverslips per condition and three independent experiments were conducted. * $p < 0.05$, ** $p < 0.01$ between SOD1^{WT} and SOD1^{G93A} astrocytes by ANOVA with Bonferroni analysis. (C) Stimulation of astrocytes with 10 μ M ATP for 30 sec results in elevated intracellular calcium levels, which returns back to baseline (after 45 secs). (D) Significantly higher intracellular calcium levels were observed in SOD1^{G93A} astrocytes in response to ATP. This response was inhibited when the cells were incubated with the Cx43 blocker GAP26 in SOD1^{WT} and SOD1^{G93A} astrocytes. Data is presented as \pm SEM with $n=8-10$ coverslips per condition and three independent experiments were conducted. * $p < 0.05$ between SOD1^{WT} and SOD1^{G93A} astrocytes and $^{***}p < 0.001$ between SOD1^{WT}/SOD1^{G93A} astrocytes and SOD1^{WT}/SOD1^{G93A} +peptide blocker by ANOVA with Bonferroni analysis.

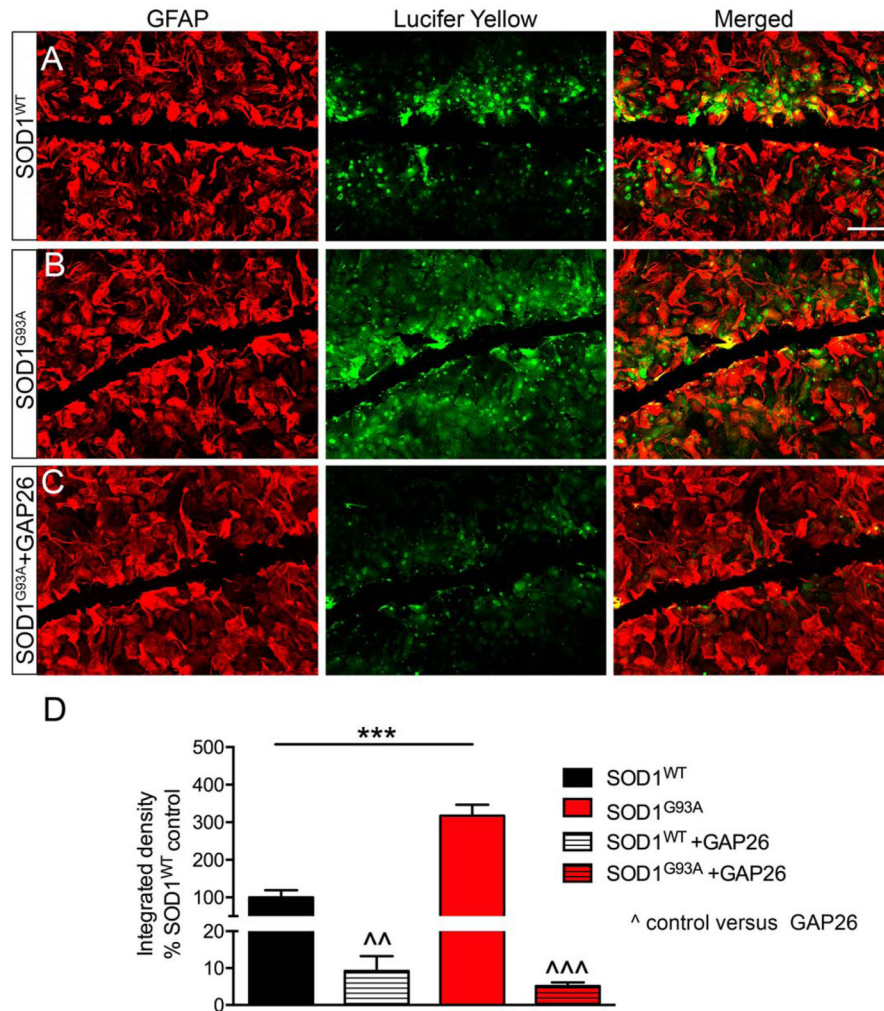


FIGURE 6.

Increased Cx43-mediated gap junction coupling occurs in SOD1^{G93A} astrocytes. Scrape-loading assay was conducted to assess gap junction coupling using Lucifer yellow (LY) dye in SOD1^{WT} astrocytes labeled with GFAP. Increased LY dye spread from the point of scrape was observed in SOD1^{G93A} astrocytes (B) when compared with SOD1^{WT} (A). (C) The spreading of LY dye was noticeably decreased when the cells were exposed to GAP26. (D) An appreciable increase in LY dye spreading and hence gap junctional coupling was observed in SOD1^{G93A} astrocytes compared to control astrocytes. When SOD1^{WT} and SOD1^{G93A} astrocytes were treated with GAP26, LY dye spreading was significantly reduced with even further decline of signal in SOD1^{G93A} astrocytes. Data is presented as \pm SEM with $n = 4-5$ coverslips per condition and three independent experiments were conducted. *** $p < 0.001$ between SOD1^{WT} and SOD1^{G93A} astrocytes, ^^ $p < 0.01$ between SOD1^{WT} and SOD1^{WT} +GAP26, ^^ $p < 0.01$ between SOD1^{G93A} and SOD1^{G93A} +GAP26 by ANOVA followed by Bonferroni test. Scale bar = 100 μ m.

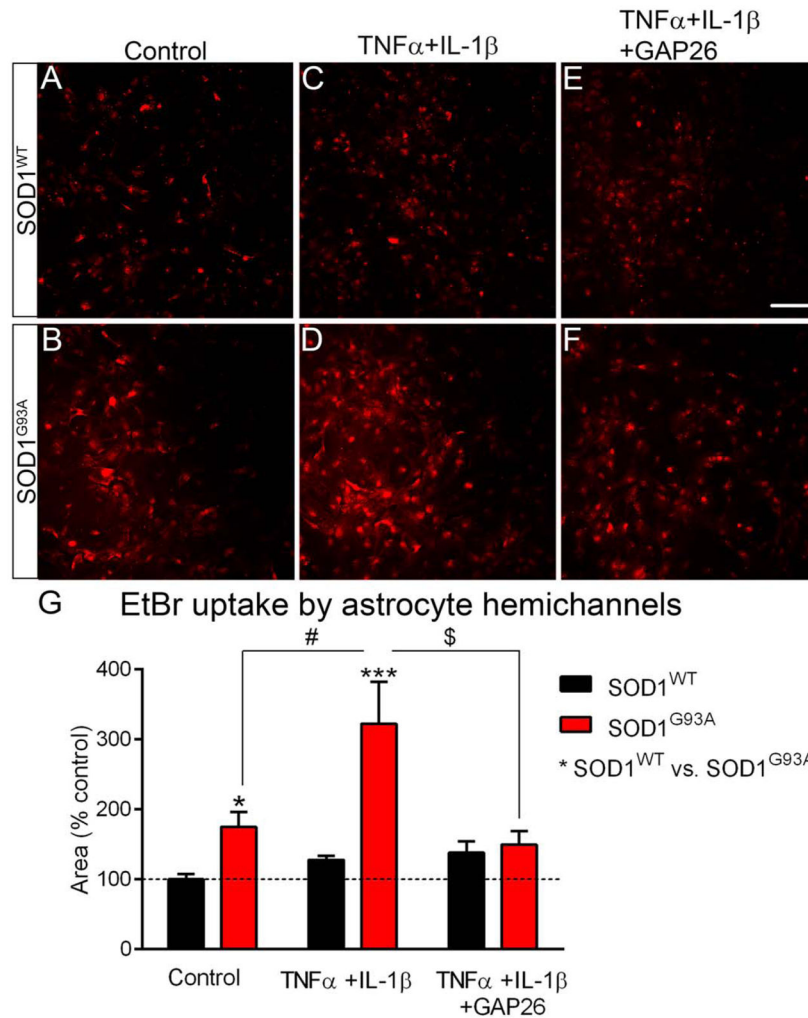


FIGURE 7. SOD1^{G93A} astrocytes have increased hemichannel activity, which is heightened when stimulated with TNF- α and IL-1 β . (A–B) Ethidium bromide (EtBr) uptake was conducted to measure the amount of hemichannel activity in SOD1^{WT} and SOD1^{G93A} astrocytes. (C–D) Astrocytes were stimulated with a cytokine mix of 10 μ M of TNF- α and 10 μ M of IL-1 β for 24 hours and the hemichannel uptake was then measured the next day. (E, F) Astrocytes from SOD1^{WT} and SOD1^{G93A} mice were co-incubated with the cytokines and GAP26. (G) A significant increase was observed in EtBr uptake in SOD1^{G93A} compared to SOD1^{WT} astrocytes and this effect was further accentuated in SOD1^{G93A} astrocytes when treated with cytokines. Notably, the inclusion of Cx43 blocker GAP26 diminishes this response back to baseline in SOD1^{G93A} astrocytes. Data is represented as \pm SEM with n=4–5 coverslips per condition and three independent experiments were conducted and analyzed using ANOVA. *p < 0.05, ***p < 0.001, SOD1^{WT} compared to SOD1^{G93A} astrocytes, #p < 0.05 SOD1^{G93A} compared SOD1^{G93A} +TNF- α +IL-1 β , \$p < 0.05 SOD1^{G93A} +TNF- α +IL-1 β compared to SOD1^{G93A} +TNF- α +IL-1 β + GAP26. Scale bar =100 μ m.

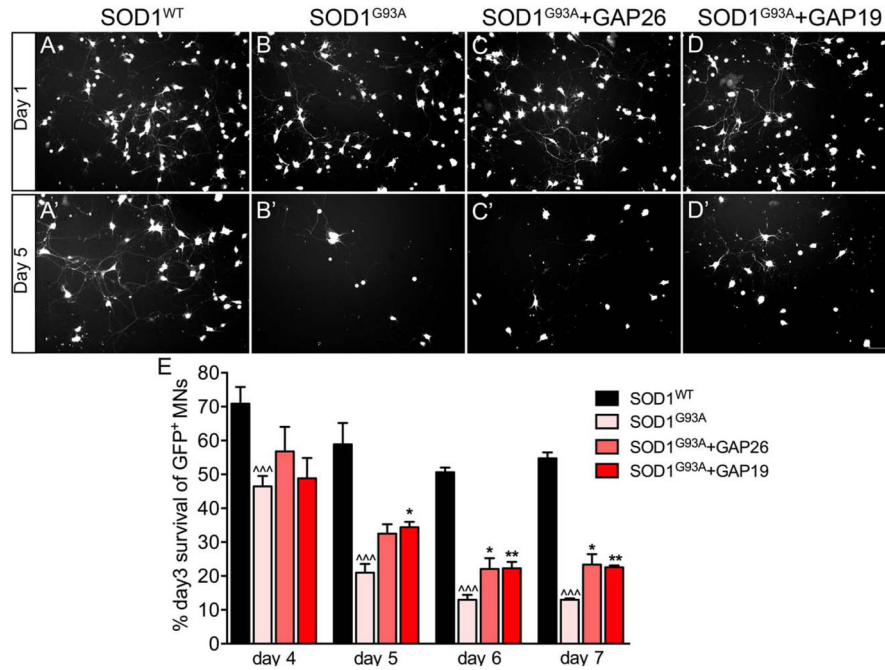


FIGURE 8.

Blocking Cx43 in astrocyte-motor neuron co-culture is neuroprotective. (A) Motor neurons were plated on top of astrocytes from SOD1^{WT} (A, A') and SOD1^{G93A} mice (B, B') and SOD1^{G93A} astrocytes treated with Cx43 hemichannel blocker GAP26 (C, C') or with Cx43 blocker GAP19 (D, D'). Compared to motor neurons plated on top of SOD1^{WT} astrocytes, motor neurons plated on top of SOD1^{G93A} astrocytes degenerated rapidly (B, B', E). However, when SOD1^{G93A} astrocytes were treated with pan Cx43 blocker GAP26 (C, C') or with Cx43 hemichannel blocker GAP19 (D, D'), significantly more motor neurons survived over time compared to untreated SOD1^{G93A} astrocytes (E). Data is represented as \pm SEM with n =4 wells per condition, per genotype and analyzed using ANOVA followed by Bonferroni post-hoc test. ^{^^^}p < 0.01 between SOD1^{WT} and SOD1^{G93A} astrocytes, *p < 0.05, **p < 0.01 with ANOVA between SOD1^{G93A} astrocytes and SOD1^{G93A} astrocytes treated with GAP19 or GAP26. Scale bar =1000 μ m.

TABLE I

Human Control and ALS Patient Samples

Category	VAB Case #	Age	Gender	Familial or Sporadic	Tissue RIN ^a	Tissue pH ^a	PMI (cr) ^b (hours)
Control	100012	81	Female	-	6.2	6.70	1-4 (approx)
Control	100036	56	Male	-	5.7	6.30	1.50
Control	110005	62	Male	-	6.6	6.38	2.75
Control	110006	68	Male	-	5.9	6.58	1.50
Control	110023	71	Female	-	4.4	5.90	2.42
5 Total							
ALS	090010	73	Male	sporadic	5.7	6.46	0.33
ALS	100018	71	Male	sporadic	6.6	6.69	7.20
ALS	100037	64	Male	sporadic	5.4	6.19	1.00
ALS	100038	57	Male	sporadic	6.4	6.39	3.38
ALS	110008	77	Male	sporadic	5.3	6.25	4.25
5 Total							

TABLE II

Human iPSCs from Control and ALS Patients

Category	Name	Age	Gender	Familial or Sporadic
Control	ciPS	-	-	-
Control	GO018	55	Female	-
Control	JH082	61	Male	-
ALS SOD1	GO013	63	Female	Familial
ALS SOD1	GO017	69	Male	Familial
ALS C9ORF72	JH033	62	Male	Familial
ALS C9ORF72	JH034	63	Female	Familial
ALS Sporadic	JH042	59	Male	Sporadic
ALS Sporadic	JH029	67	Male	Sporadic
ALS Sporadic	JH058	56	Female	Sporadic